PCCP

Accepted Manuscript

ROYAL SOCIETY OF CHEMISTRY

www.rsc.org/pccp

4/2/2014

Time-Resolved Fluorescence Spectroscopy Study of Excited State Dynamics of Alkyl- and Benzo-Substituted Triphyrin(2.1.1)

Yusuke Iima,[a] Daiki Kuzuhara,[b] Zhao-Li Xue,[b] Seiji Akimoto,[a,c] Hiroko Yamada[b*] and Keisuke Tominaga[a,c,*]

[a]Graduate School of Science, Kobe University, 1-1 Rokkodai-cho, Nada, Kobe 657-8501, Japan

[b]Graduate School of Materials Science, Nara Institute of Science and Technology, NAIST, 8916-5 Takayama, Ikoma, Nara 630-0192, Japan

[c]Molecular Photoscience Research Center, Kobe University, 1-1 Rokkodai-cho, Nada, Kobe 657-8501, Japan

*Corresponding authors

E-mail addresses: hyamada@ms.naist.jp (H. Yamada), tominaga@kobe-u.ac.jp (K. Tominaga)

Abstract

We have investigated the photophysical properties of alkyl-substituted triphyrin(2.1.1) (ATp) and benzotriphyrin(2.1.1) (BTp) by steady-state and time-resolved fluorescence spectroscopy. We focused on the effect of NH proton tautomerization, planarity of the macrocycles, and substituents on these properties. The fluorescence quantum yields (Φ_y) of ATp did not depend on solvent viscosity, whereas those of BTp increased with solvent viscosity, reaching a maximum value of 0.17 in paraffin. Interestingly, analyzing Φ_y showed that the non-radiative rate constant of BTp decreased sharply as the solvent viscosity increased. These results suggest that the substituted phenyl groups play a crucial role in suppressing molecular distortion, thus leading to decreased non-radiative relaxation in triphyrin(2.1.1). The hydrogen bond formed in the inner cavity potentially contributes to the suppression of the structural distortion, whereas the pyrrole rings in the macrocycle are close, as in porphycene.

I. Introduction

There has been a considerable interest in the photophysical properties of porphyrinoids because of their potential applications in dyes, nonlinear optics, and photonic devices.[1-3] To design porphyrinoids with excellent luminescence properties, it is necessary to understand the non-radiative relaxation processes to gain insight into the relationship between the photophysical properties and structural characteristics, such as the substituents, planarity, and macrocyclic geometry. Numerous studies have suggested that the non-radiative relaxation of porphyrin is governed by several structural features, including the out-of-plane distortion of the porphyrin ring caused by bulky substituent groups, and the insertion of metal into the cavity, which enhances internal conversion and intersystem crossing.[4-7] The enhanced internal conversion is interpreted as arising from an enhanced Franck-Condon factor associated with a structural reorganization in the excited state.[5] The non-planarity of porphyrinoids in the excited state is discussed in detail in Refs. 8 and 9. In addition, Waluk *et al*. suggested that NH proton tautomerization contributes to the non-radiative relaxation of porphycene because the neighboring nitrogen atoms are close together.[10,11] They showed that NH proton tautomerization distorts the porphycene macrocycle due to repulsion between the neighboring pyrroles.

The porphyrin derivative free-base triphyrin(2.1.1) has recently been synthesized and shows very short fluorescence lifetimes.[12-14] Free-base triphyrin(2.1.1) has a non-planar conformation similar to that of less fluorescent porphyrins and a short NH···N distance similar to that in porphycene. Therefore, it is not clear whether the non-planarity or the NH proton tautomerization is more important for the non-radiative relaxation. According to Kim *et al.*,[15] the fluorescence lifetime of subpyriporphyrin depends on temperature and viscosity; it is 8 ps at room temperature and 458 ps at 77 K in a viscous environment. This arises from the NH proton tautomerization in the excited state, as in porphycene. In contrast, we have suggested that in benzotriphyrin(2.1.1) (BTp), the molecular distortion causes the non-radiative relaxation in the excited state, because BTp shows no NH proton tautomerization.[12] Sung et al. investigated the photophysical properties of two types of triphyrins, bicycle[2.2.2]octadiene (BCOD) triphyrin(2.1.1) and BTp and concluded that the main factor that affects the excited state lifetime is peripheral fused ring moieties.[16]

In this work, we investigated the roles of the substituent groups and the NH proton tautomerization in the non-radiative relaxation of triphyrin(2.1.1) by steady-state and time-resolved fluorescence spectroscopy of alkyl-substituted triphyrin(2.1.1) (ATp) and BTp (Figure 1). Both triphyrins show a prominent downfield shift of the inner

protons in ^{1}H-NMR spectrum, reflecting a strong hydrogen bond in the small cavity.[13,14] We examined the effect of the substituents by measuring the fluorescence quantum yields (Φ_y) in various solvents. Furthermore, we used steady-state fluorescence anisotropy to investigate the NH proton tautomerization in the excited state, and the contribution of the NH proton tautomerization to non-radiative relaxation. Intriguingly, the dependence of fluorescence quantum yield on viscosity differed between ATp and BTp. Our results provide further insight into the role of the substituent groups in the non-radiative relaxation dynamics of triphyrin(2.1.1).

II. Experimental

ATp and BTp were synthesized according to Refs. 13 and 14, respectively, and were purified by recrystallization ($CHCl_3$/water for ATp and $CHCl_3$/MeOH for BTp) and HPLC. The purity was checked by confirming that the fluorescence decays were described by a single component. All solvents used to prepare the liquid samples were spectral grade. Paraffin and 2-methyltetrahydrofuran (2MTHF) were purified before use according to the procedures in Ref. 17. For the fluorescence spectral measurements, all solutions were prepared at concentrations where the absorbance at the Q-like band around 550 nm for ATp and 590 nm for BTp was below 0.1. The fluorescence quantum

yield of ATp was measured with a fluorospectrometer (FP-6500, JASCO) and that of BTp was measured with an absolute quantum yield measurement system (C9920-02, Hamamatsu Photonics). The excitation wavelengths were 340 and 410 nm for ATP and BTp, respectively. For ATp, rhodamine 6G (Exciton), which was purified by recrystallization ($CHCl_3$/MeOH), was used as a reference (Φ_y^R = 0.98 in CH_2Cl_2; estimated by the absolute PL quantum yield measurement method described above). Φ_y is given by

$$\Phi_y = \Phi_y^R \cdot \frac{n^2}{n_R^2} \cdot \frac{\int F(\lambda_F) d\lambda_F}{\int F_R(\lambda_F) d\lambda_F} \quad (1)$$

where the subscript and superscript *R* refer to the reference solution, *n* is the refractive index, and $F(\lambda_F)$ is the fluorescence spectrum. The fluorescence spectra were corrected by the method published by Valeur.[18] Fluorescence decay was measured with a time-correlated single-photon counting system. The output from a mode-locked Ti:sapphire laser (Tsunami, Spectra-Physics) was passed through a pulse picker operating at 2.9 MHz, and the second harmonic (400 nm) was then used to excite the samples. The full width at half-maximum of the instrumental response function was about 60 ps. The fluorescence decay curve was fitted by a convolution of the instrumental response function and a sum of exponential functions. The radiative and non-radiative rate constants are estimated by

$$\Phi_y = \frac{k_r}{k_r + k_{nr}} = k_r \cdot \tau \quad (2)$$

where k_r and k_{nr} are the radiative and the non-radiative rate constants, respectively, and τ is the fluorescence lifetime.

III. Results and Discussion

III. A. Steady-State Absorption Spectra and Fluorescence Spectra

Figure 2 shows the absorption spectra of ATp and BTp measured in eight solvents (*n*-hexane (C6), THF, $CHCl_3$, DMSO, MeCN, EtOH, MeOH, and ethylene glycol (EG)). The oscillator strengths of the transition bands calculated by time-dependent density functional theory (TD-DFT) with a basis set of cc-pVDZ are also shown. ATp exhibits intense B-like (340 nm) and structureless Q-like bands, whereas BTp shows clear B- (414 nm) and Q-like (580 nm) absorption bands in C6, similar to porphyrin.[19,20] The fluorescence spectra in Figure 3 show the emission band attributed to the $S_1 \rightarrow S_0$ transitions as a mirror image of the Q-like bands. It has been reported that the magnetic circular dichroism (MCD) spectrum shows coupled pairs of oppositely signed Gaussian-shaped bands for BTp, similar to those observed for the Q and B bands of low-symmetry porphyrins.[13] The TD-DFT results agreed well with the experimentally

obtained absorption and MCD spectra, except for the relative peak positions. In the case of BTp, the observed band structures were qualitatively consistent with those predicted by the Gouterman four-orbital model of the 14π system, which is similar to the porphyrin 18π system.[19,20] However, the oscillator strengths for ATp showed many transitions in the Q-like band. The energy level diagram calculated by TD-DFT (Figure 4) shows that close, low-lying molecular orbitals below the HOMO, such as HOMO-1, HOMO-2, and HOMO-3, contribute to the electronic transitions to the LUMO, resulting in many excited states, as observed in BCOD triphyrin(2.1.1).[16]

The spectral shapes of the absorption and fluorescence of BTp were independent of the polarities and the protic properties of the solvents. The fluorescence spectra of BTp contained the $S_1 \rightarrow S_0$ emission band as a mirror image of the absorption spectra, which had similar peak wavelengths irrespective of the solvent polarity. In contrast, the ATp absorption band at 490 nm increased and that at 550 nm decreased (indicated by arrows) in polar protic solvents, such as MeOH and EG. Because the TD-DFT calculation predicted several electronic transitions in this wavelength region, the oscillator strengths of these transitions were expected to change in protic solvents. This suggests that the ATp macrocycle may be distorted in protic solvents, because of hydrogen bonding between the inner nitrogen atoms and the hydroxyl protons of the

solvent molecules (R-OH···N). Furthermore, we assume that BTp is not distorted in protic solvents because the phenyl groups, especially at the *meso*-CH_2 carbons, prevent distortion.

We investigated the internal conversion upon photoexcitation from the upper excited states, S_n, to the S_1 state in the fluorescence excitation spectra. In Figure 5, we compare the absorption and excitation spectra of ATp and BTp in CH_2Cl_2. Because the excitation spectra corresponded well to the absorption spectra for both ATp and BTp, we conclude that internal $S_n \rightarrow S_1$ conversion is much faster than the S_1 lifetime. For BTp, we confirmed this by using time-resolved fluorescence spectroscopy, which showed that the internal conversion from the Soret states to the S_1 state was complete within 150 fs, which is much faster than the S_1 lifetime of 140 ps.[12]

III. B. Viscosity Dependence of Fluorescence Quantum Yields and Lifetimes

In our previous time-resolved fluorescence study of BTp, we proposed that the excited state internal conversion of $S_1 \rightarrow S_0$ is governed not by the NH proton tautomerization in the excited state, as it is in porphycene, but by the non-planarity of the macrocycle.[12] According to Sung *et al.*,[16] the S_1 lifetime of BCOD triphyrin(2.1.1) in toluene was shortened to 6 ps by introducing the bulky BCOD group at β carbons. However, the

lifetimes of BCOD triphyrin(2.1.1) and BTp are the same, namely, 3.2 ns, at liquid nitrogen temperature, whereas the lifetime of BCOD triphyrin(2.1.1) is 180 ps in toluene, which is 1/30th that of BTp at room temperature. They concluded that these findings suggest that the flexible motion of the triphyrin(2.1.1) macrocycle ring such as doming and ruffling is restricted by the fused moieties.

We investigated the role of *meso*-substituted groups in the fluorescence properties by comparing ATp and BTp. To assess the effect of the substituents on the fluorescence properties, we examined the dependence of fluorescence quantum yield and fluorescence lifetime on solvent viscosity. To eliminate the interactions between the solute and solvent, such as hydrogen bonding, π-π and dipole-dipole interactions, we used hydrocarbons with various alkyl chain lengths. Table 1 shows the values of Φ_y, τ, k_r, and k_{nr} for ATp and BTp. The viscosity dependence of the fluorescence decays, k_r, and k_{nr} are shown in Figures 6 and 7. For ATp, both k_r and k_{nr} showed negligible dependence on the solvent viscosity. In contrast, for BTp, k_{nr} decreased to 1/10th the initial value as the solvent viscosity increased from C5 to paraffin, whereas k_r was the same within experimental error, regardless of the solvent. The viscosity dependence of BTp shows that hindering molecular distortion in the excited states suppresses the non-radiative relaxation in viscous solvents. Furthermore, the ATp and BTp results

suggest that the non-radiative relaxation is suppressed by the phenyl groups at both β- and *meso*-carbons. Although X-ray structures show that both the triphyrins are nearly planar (Figure 8),[13,14] it is reasonable to expect for BTp that the planarity is maintained in the solutions by the size restriction and π-π interactions of the *meso*-substituted phenyl rings.

X-ray crystal structure analysis revealed that both free-base ATp and free-base BTp have nearly planar structures,[13,14] but that the pyrrole ring between the two methyne carbon atoms is relatively free to undergo flip-flop motion. By inserting a metal ion into ATp and BTp, however, the three pyrole rings in the macrocycle remain as a dome structure.[14,21-24] The reason is that, if we view the three pyrrole rings as an isosceles triangle, the two pyroles forming the base are fixed to each other via a hydrogen bond but the one at the apex can flip-flop freely. This suggests that the tryphirin(2.1.1) macrocycle is structurally flexible and that its planarity can change in solution depending on solvent viscosity and substituent groups.

III. C. Effect of NH Proton Tautomerization

Next, we discuss the effect of the NH proton tautomerization in the excited state, which contributes to the photophysical properties of several porphyrinoids.[10,11,15] According to

Waluk *et al.*,[10,11] the NH proton tautomerization in the excited state contributes to the non-radiative relaxation of porphycene, because the cavity of the macrocycle is small. As with porphycene, the NH proton tautomerization of triphyrin(2.1.1) may contribute to Φ_y because of the small inner cavity. To assess the contribution, we estimated Φ_y of deuterated and protonated (cationic) triphyrin(2.1.1). Table 2 shows the values of Φ_y and the fluorescence lifetime in MeOD and 10% trifluoroacetic acid (TFA)/THF (1:9 v/v), and also in the reference solvents MeOH and THF. Figure 9 shows the absorption and fluorescence spectra of ATp and BTp in TFA/THF. Unlike porphycene,[11] both ATp and BTp have values of Φ_y that are similar in MeOD and MeOH, even though the neighboring N···N distances are short (ATp: 2.552 Å; BTp: 2.573 Å).[13,14] We also obtained the fluorescence anisotropy spectra to determine changes in the transition dipole moment caused by NH proton tautomerization in the excited state. For porphycene, the anisotropy value for $S_1 \rightarrow S_0$ decreased, even when the rotational relaxation was hindered, as observed in glassy solvents.[25] Figure 10 shows that both ATp and BTp have an anisotropy value of about 0.4 for the $S_1 \rightarrow S_0$ transition, indicating that NH proton tautomerization did not occur in glassy solvents, which is consistent with the Φ_y measurements in MeOD. Based on these results, we conclude that NH proton tautomerization in the excited states is less important to the

non-radiative relaxation of triphyrin(2.1.1).

Whereas repulsion between hydrogen atoms opposite each other in the cavity of porphycene is important for its non-radiative relaxation, the repulsion may play a less important role in the triphyrin(2.1.1) cavity. Because triphyrin(2.1.1) has one hydrogen in the cavity, the strong NH···N hydrogen bond could help to suppress the molecular distortion instead. When triphyrin(2.1.1) is cationized by TFA, Φ_y decreases sharply, as shown in Table 2. In this case, the repulsion between the inner three protons increased and triphyrin(2.1.1) became distorted. The triphyrin(2.1.1) distortion may lead to a decrease in Φ_y as it does in porphyrin.[4-7]

IV. Summary

We have investigated the role of substituent groups and NH proton tautomerization in the non-radiative relaxation of triphyrin(2.1.1) by studying ATp and BTp with steady-state and time-resolved fluorescence spectroscopy. The fluorescence lifetime measurements showed that the non-radiative relaxation in BTp was strongly suppressed in viscous solvents. In contrast, the fluorescence lifetime of ATp did not show viscosity dependence. From these results, we conclude that molecular distortion is a major factor in suppressing the non-radiative relaxation, and that the phenyl substituents in

triphyrin(2.1.1) may contribute to this suppression. Moreover, the fluorescence anisotropy and Φ_y measurements in MeOD suggest that NH proton tautomerization did not occur in the excited state lifetime, in contrast to porphycene. Based on these observations, we propose that structural distortion is a cause of the increase in non-radiative relaxation in triphyrin(2.1.1) and that the hydrogen bond formed in the inner cavity may suppress the distortion, unlike in porphycene.

4/2/2014

V. Reference

1. G. de la Torre, P. Vazquez, F. Agulló-López, T. Torres, *Chem. Rev.* **2004**, 104, 3723.

2. C. G. Claessens, D. Gonzáles-Rodriguez, T. Torres, *Chem. Rev*. **2002**, 102, 835.

3. T. Torres, *Angew. Chem., Int. Ed.* **2006**, 45, 2834.

4. S. Gentemann, C. J. Medforth, T. Ema, N. Y. Nelson, K. M. Smith, J. Fajer, D. Holten, *Chem. Phys. Lett.* **1995**, 245, 441.

5. S. Gentemann, C. J. Medforth, T. P. Forsyth, D. J. Nurco, K. M. Smith, J. Fajer, D. Holten, *J. Am. Chem. Soc*. **1994**, 116, 7363.

6. I. V. Sazanovich, V. A. Galievsky, A. Hoek, T. J. Schaafsma, V. L. Malinovskii, D. Holten, V. S. Chirvony, *J. Phys. Chem. B* **2001**, 105, 7818.

7. V. S. Chirvony, A. Hoek, V. A. Galievsky, I. V. Sazanovich, T. J. Schaafsma, D. Holten, *J. Phys. Chem. B* **2000**, 104, 9909.

8. T. Kojima, T. Nakanishi, R. Harada, K. Ohkubo, S. Yamauchi and S. Fukuzumi, *Chem. Eur. J.* **2007**, 13, 8714.

9. T. Nakanishi, K. Ohkubo, T. Kojima, S. Fukuzumi, *J. Am. Chem. Soc.* **2009**, 131, 577.

10. A. L. Sobolewski, M. Gil, J. Dobkowski, J. Waluk, *J. Phys. Chem. A* **2008**, 113,

7714.

11. M. Gill, J. Dobkowski, G. W.-Salyga, N. Urbanska, P. Fita, C. Radzewicz, M. Pietraszkiewicz, P. Borowicz, D. Marks, M. Glasbeek, J. Waluk, *J. Am. Chem. Soc.* **2010**, 132, 13472.

12. Y. Iima, D. Kuzuhara, Z. L. Xue, H. Uno, S. Akimoto, H. Yamada, K Tominaga, *Chem. Phys. Lett.* **2011**, 513, 67.

13. Z. L. Xue, Z. Shen, J. Mack, D. Kuzuhara, H. Yamada, T. Okujima, N. Ono, X. Z. You, N. Kobayashi, *J. Am. Chem. Soc.* **2008**, 130, 16478.

14. D. Kuzuhara, H. Yamada, Z. L. Xue, T. Okujima, S. Mori, Z. Shen and H. Uno, *Chem. Comm.* **2011**, 47, 722.

15. K. S. Kim, J. M. Lim, R. Mysliborski, M. Pawlicki, L. L.-Grazynski, D. Kim, *J. Phys. Chem. Lett.* **2011**, 2, 477.

16. Y. M. Sung, J. M. Lim, Z. L. Xue, Z. Shen, D. Kim, *Chem. Comm.* **2011**, 47, 12618.

17. W. L. F. Armarego, C. L. L. Chai, *Purification Laboratory Chemicals*, sixth edition, Elsevier Inc. **2009**.

18. B. Valeur, *Molecular fluorescence Principles and applications*, WILEY-VCH, **2002**, 158.

19. M. Gouterman, *J. Chem. Phys.* **1959**, 30, 1139.

20. M. Gouterman, *J. Mol. Spec.* **1961**, 6, 138.

21. Z. L. Xue, J. Mack, H. Lu, L. Zhang, X. Z. You, D. Kuzuhara, M. Stillman, H. Yamada, S. Yamauchi, N. Kobayashi, Z. Shen, *Chem. Eur. J.* **2011**, 17, 4396.

22. Z. L. Xue, D. Kuzuhara, S. Ikeda, T. Okujima, S. Mori, H. Uno and H. Yamada, *Inorg. Chem.* **2013**, 52, 1688.

23. Z. L. Xue, D. Kuzuhara, S. Ikeda, Y. Sakakibara, K. Ohkubo, N. Aratani, T. Okujima, H. Uno, S. Fukuzumi and H. Yamada, *Angew. Chem. Int. Ed.* **2013**, 52, 7306.

24. D. Kuzuhara, Z. L. Xue, S. Mori, T. Okujima, H. Uno, N. Aratani and H. Yamada, *Chem. Comm*. **2013**, 49, 8955.

25. J. Waluk, E. Vogel, *J. Phys. Chem.* **1994**, 98, 4530.

4/2/2014

Table 1. Fluorescence quantum yield, fluorescence lifetime, and radiative and non-radiative rate constants of ATp and BTp[1]

	Solvent	η / cP	Φ_y	τ /ns [2]	k_r /ns^{-1} [3]	k_{nr}/ns^{-1} [3]
ATp	*n*-pentane (C5)	0.225	1.0×10^{-4}	0.024	0.005	42
	n-hexane (C6)	0.299	1.2×10^{-4}	0.031	0.004	32
	n-heptane (C7)	0.391	1.4×10^{-4}	0.026	0.005	39
	n-octane (C8)	0.515	1.5×10^{-4}	0.033	0.005	31
	n-dodecane (C12)	1.37	0.9×10^{-4}	0.029	0.003	35
	n-pentadecane (C15)	2.57	1.2×10^{-4}	0.026	0.005	38
	Paraffin	91.3	1.7×10^{-4}	0.035	0.004	29
BTp	C5	0.225	0.010	0.16	0.05	6.2
	C6	0.299	0.016	0.20	0.08	4.9
	C7	0.391	0.019	0.24	0.08	4.1
	C8	0.515	0.028	0.29	0.10	3.3
	C12	1.37	0.050	0.51	0.10	1.9
	C15	2.57	0.070	0.70	0.10	1.3
	Paraffin	91.3	0.17	1.47	0.12	0.6

[1]All measurements are performed at room temperature (293 K).

[2]Obtained by fitting fluorescence decay with a single exponential function.

[3]Determined from the relationship between Φ_y and τ (equation 2).

4/2/2014

Table 2. Fluorescence quantum yield, fluorescence lifetime, and radiative and non-radiative rate constants of ATp and BTp[1]

	Solvent / phase	η / cP	Φ_y	τ /ns [2]	k_r/ns^{-1} [3]	k_{nr}/ns^{-1} [3]
ATp	CH_2Cl_2	0.425	5×10^{-5}	0.035	0.001	29
	DMSO	2.00	2×10^{-5}	0.031	0.001	32
	MeOH	0.555	2×10^{-4}	0.034	0.006	29
	MeOD	0.550	1×10^{-4}	0.035	0.003	29
	THF	0.480	9×10^{-5}	0.034	0.003	29
	TFA 10%/THF	-	4×10^{-6}	<0.03	>0.0001	<33
BTp	CH_2Cl_2	0.425	0.005	0.078	0.06	13
	DMSO	2.00	0.012	0.26	0.05	3.8
	MeOH	0.555	0.007	0.090	0.08	11
	MeOD	0.550	0.007	0.087	0.08	11
	THF	0.480	0.008	0.130	0.06	7.6
	TFA 10%/THF	-	0.003	0.044	0.07	23

[1]All measurements are performed at room temperature (293 K).

[2]Obtained by fitting fluorescence decay with single exponential function.

[3]Determined from the relationship between Φ_y and τ (equation 2).

Figure captions

Figure 1. Structure of ATp (left) and BTp (right).

Figure 2. Absorption spectra in C6, THF, $CHCl_3$, DMSO, MeCN, EtOH, MeOH, and EG of (a1) ATp and (a2) BTp. Oscillator strengths calculated by using the TD-DFT method with the B3LYP/cc-pDVZ basis set for (b1) ATp and (b2) BTp. The inset in (a1) compares the absorption spectra of C6 and EG. Arrows indicate spectral changes in MeOH and EG.

Figure 3. Fluorescence spectra in C6, THF, $CHCl_3$, DMSO, MeCN, EtOH, MeOH, and EG of (c1) ATp and (c2) BTp. For ATp λ_{ex} = 340 nm and for BTp λ_{ex} = 414 nm.

Figure 4. Frontier molecular orbital diagram and contour plots of occupied and virtual orbitals of ATp (left) and BTp (right), calculated by using the TD-DFT method with the B3LYP/cc-pDVZ basis set.

Figure 5. Excitation (solid line) and absorption (dotted line) spectra of ATp (upper) and BTp (lower) in CH_2Cl_2. The detection wavelength was 600 nm for both ATp and BTp. The asterisk indicates the Raman band of CH_2Cl_2.

Figure 6. Fluorescence decay of ATp (upper) and BTp (lower) in C5 (red), C6 (orange), C7 (yellow), C8 (light green), C12 (green), C15 (light blue), and paraffin (blue). λ_{ex} = 400 nm, for ATp λ_{em} = 560 nm, and for BTp λ_{em} = 590 nm. The dashed line is the

instrumental response function.

Figure 7. Viscosity dependence of k_r and k_{nr} for ATp (upper) and BTp (lower). Hydrocarbons of various lengths are used as solvents: C5, C6, C7, C8, C12, C15, and paraffin.

Figure 8. X-ray crystal structures of ATp (left) and BTp (right):[13,14] (a) top view and (b) side view.

Figure 9. Normalized absorption and fluorescence spectra of ATp (upper) and BTp (lower) in 10% TFA/THF solution. For ATp λ_{ex} = 340 nm and for BTp λ_{ex} = 410 nm.

Figure 10. Fluorescence excitation spectra (a) and anisotropy (b) of ATp (left) and BTp (right) measured at 123 K in 2MTHF. For ATp λ_{em} = 560 nm and for BTp λ_{ex} = 590 nm.

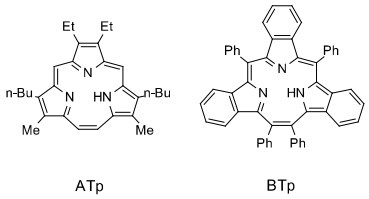

ATp BTp

Figure 1.

4/2/2014

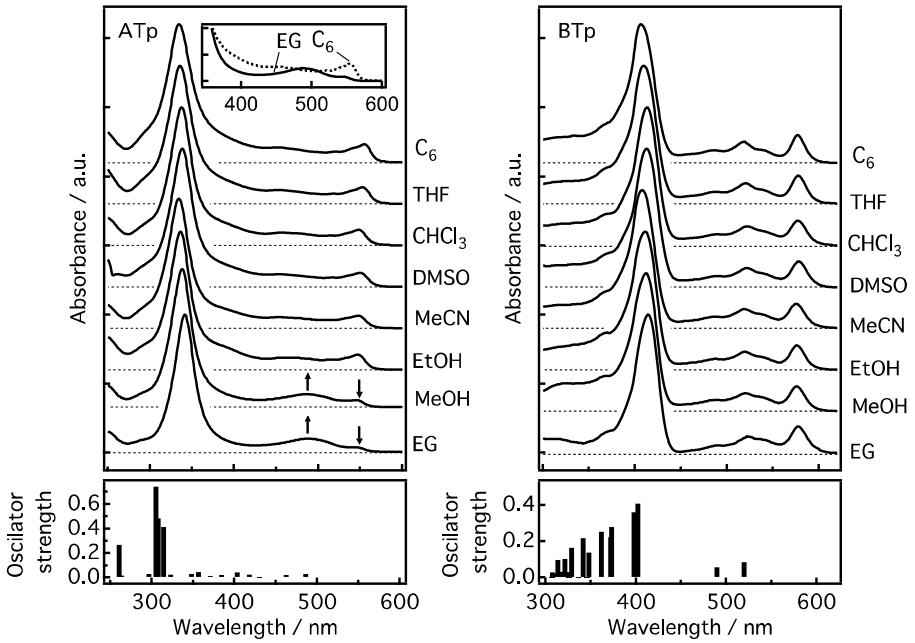

Figure 2.

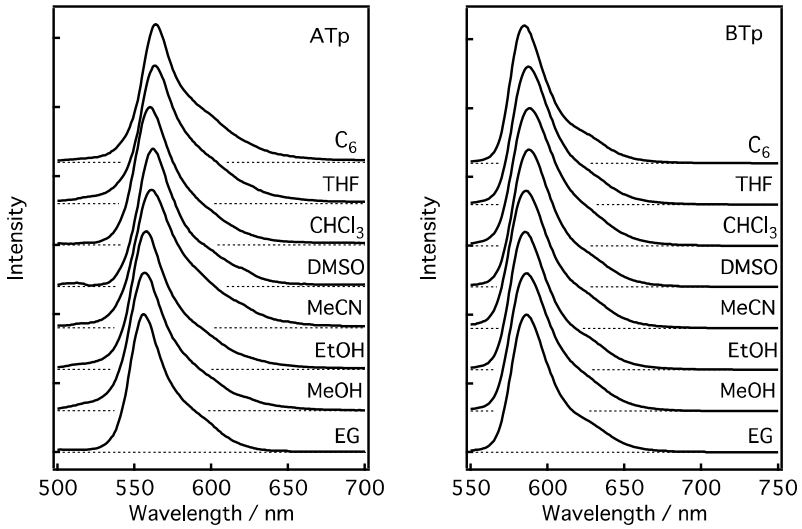

Figure 3.

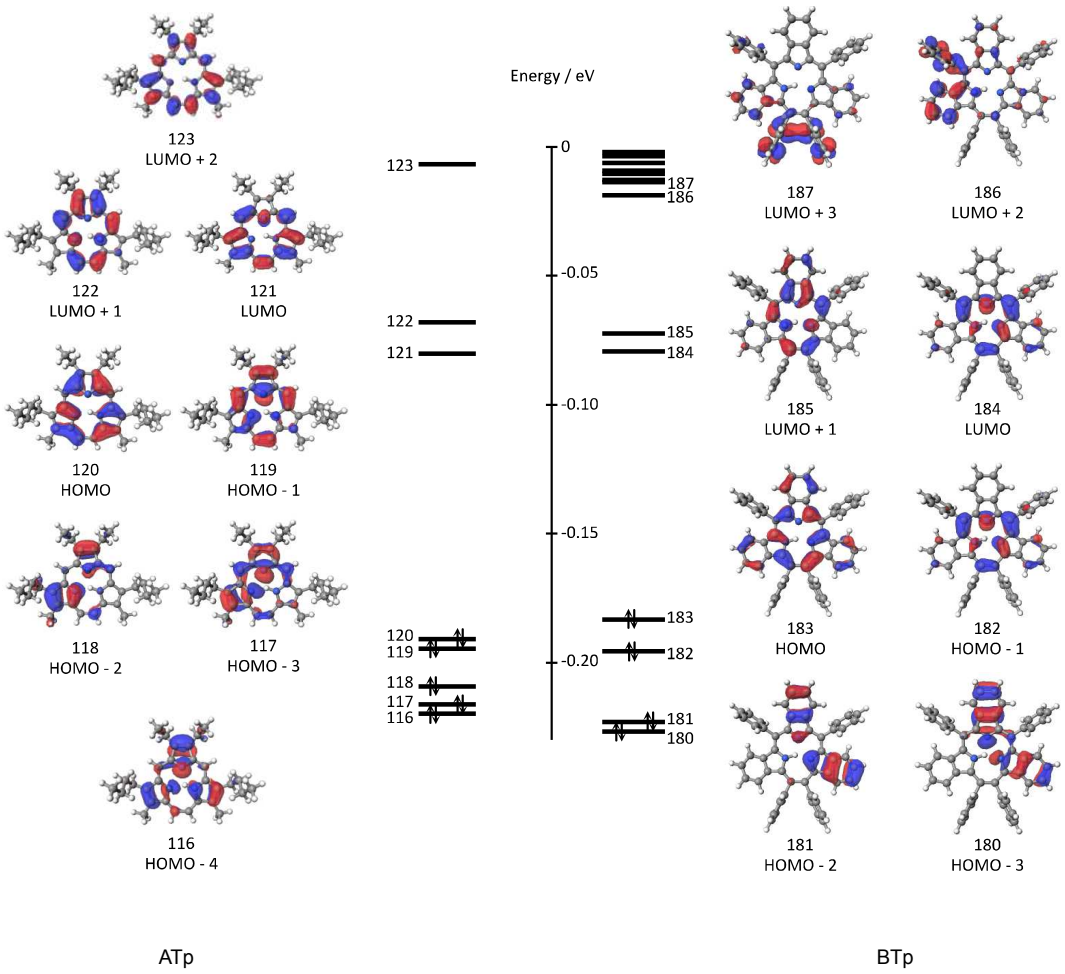

Figure 4.

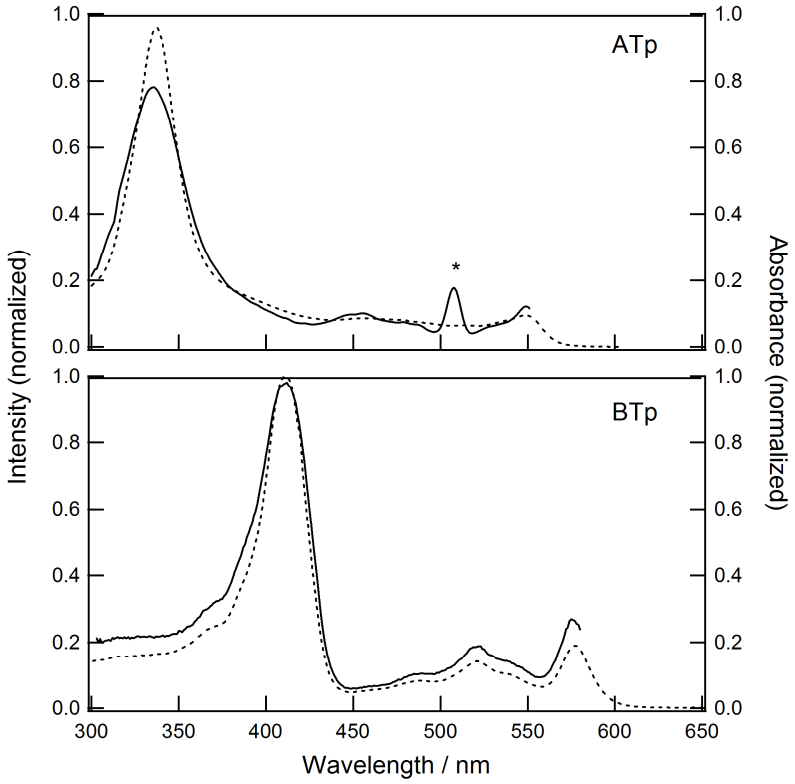

Figure 5.

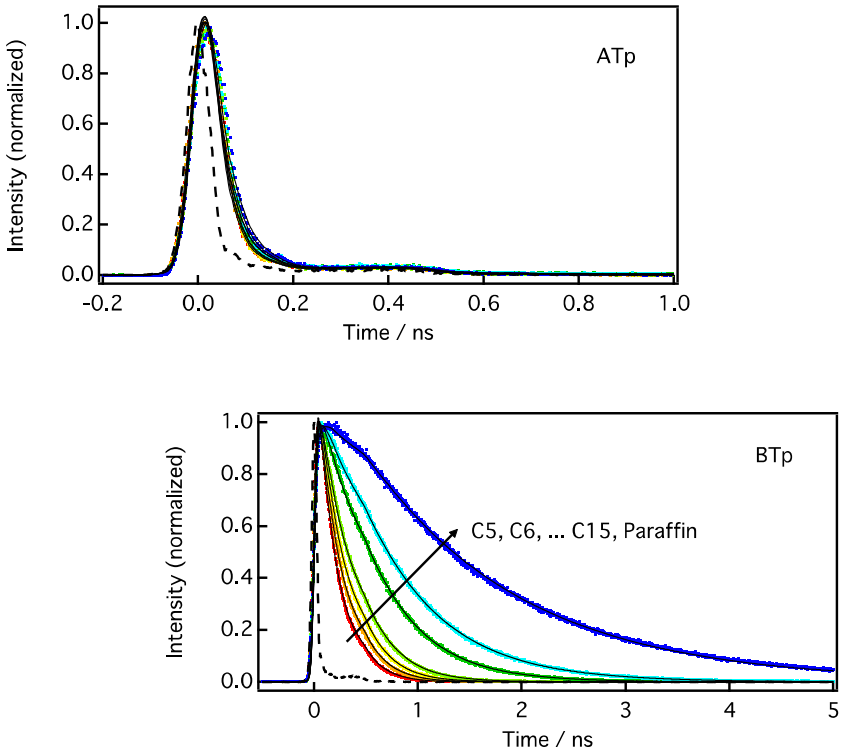

Figure 6.

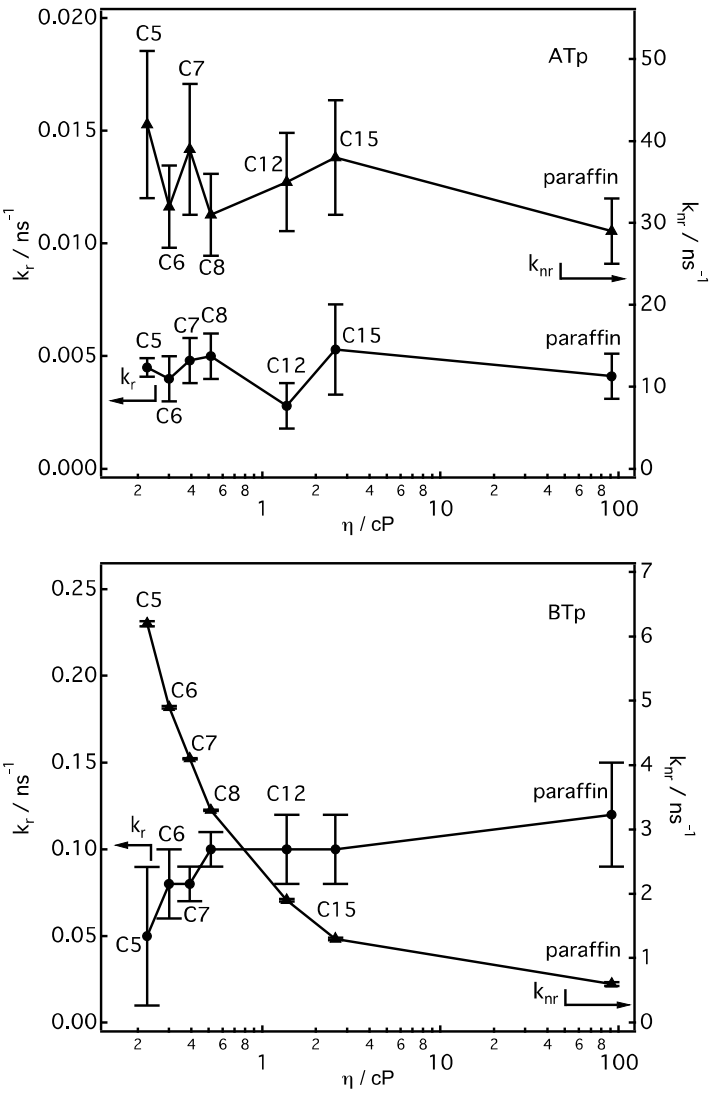

Figure 7

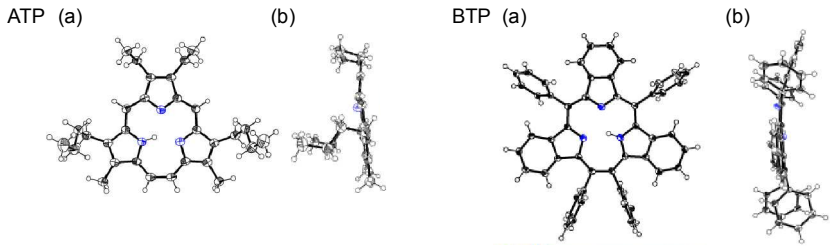

Figure 8.

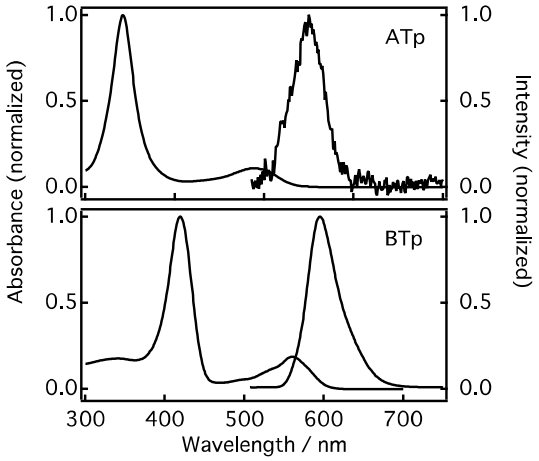

Figure 9.

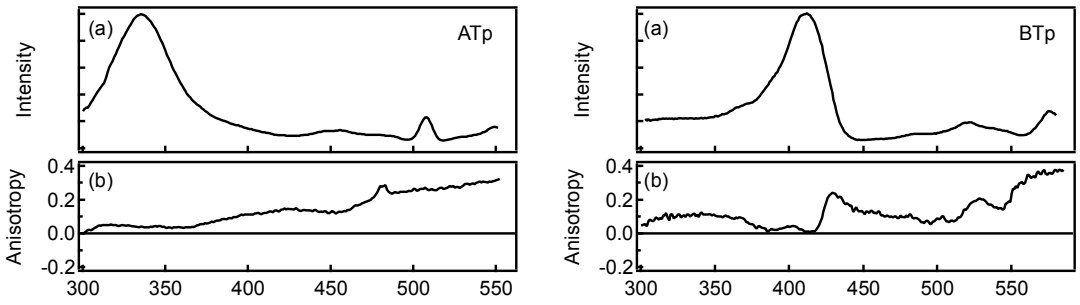

Figure 10.